Supporting Information

High-Performance Photovoltaic Hydrogen Sensing Platform with Light-Intensity Calibration Module

Hyeonghun Kim[†], Woochul Kim[†], Ryeri Lee[†], Sungjun Cho[†], Jiyoon Park[†], Yusin Pak*[‡] and Gun Young Jung*[†]

[†] School of Materials Science and Engineering, Gwangju Institute of Science and Technology (GIST), 123 Chemdangwagi-ro, Buk-gu, Gwangju 61005, Republic of Korea.

[‡] Sensor System Research Center (SSRC), Korea Institute of Science and Technology (KIST), Seoul 02792, Republic of Korea.

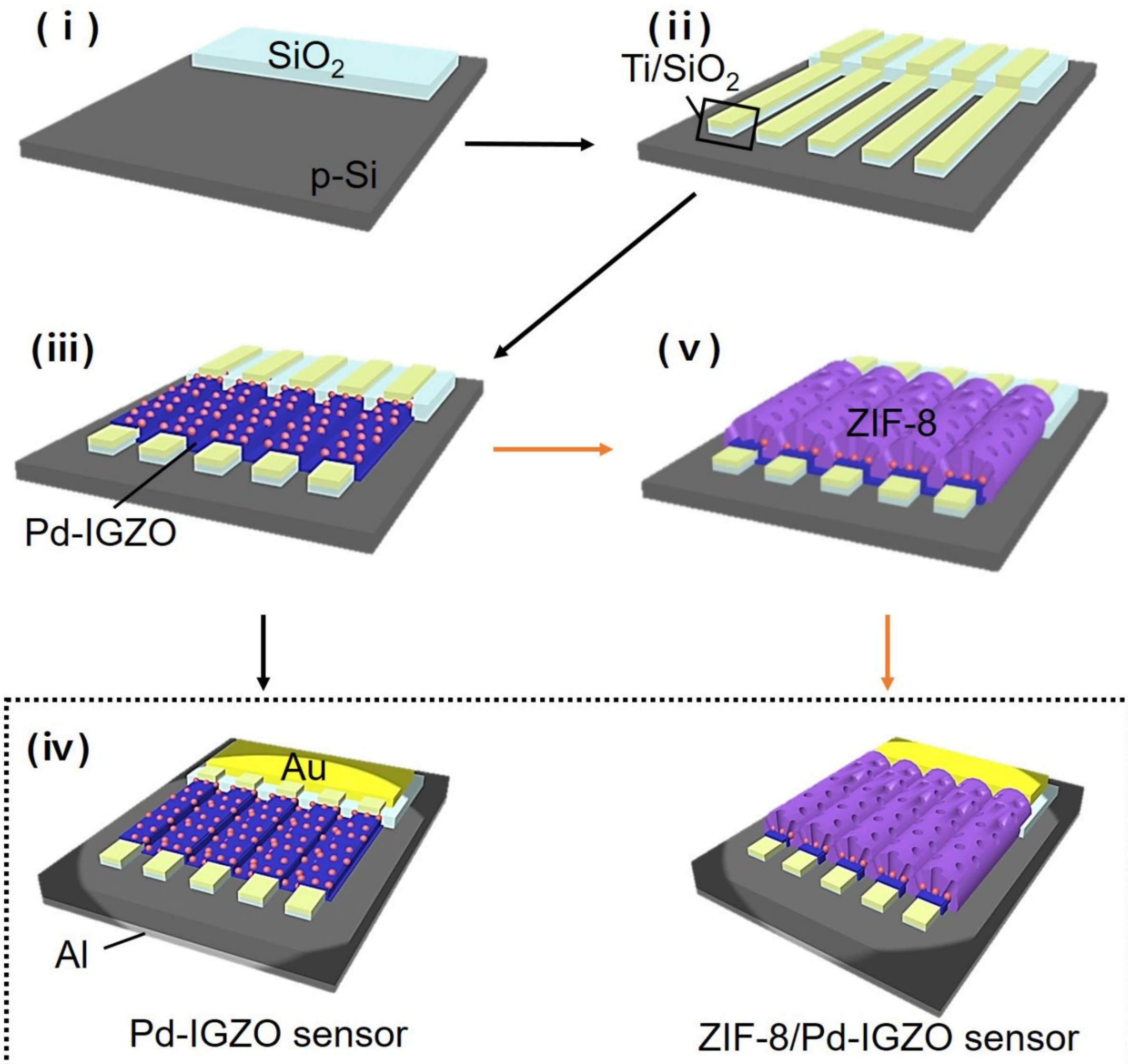

Figure S1. Fabrication procedure of Pd-IGZO sensor and ZIF-8/Pd-IGZO sensor. (i) Deposition of SiO_2 layer on an Si substrate. (ii) Construction of finger-type Ti (30 nm)/SiO_2 (50 nm) electrodes. (iii) Subsequent deposition of IGZO (50 nm) and Pd catalysts (0.5 nm). (iv) Creating Au contact to assemble the entire Ti finger electrodes, and Al bottom electrode as a back contact. (v) Coating of microporous ZIF-8 layer on the Pd-decorated IGZO layer.

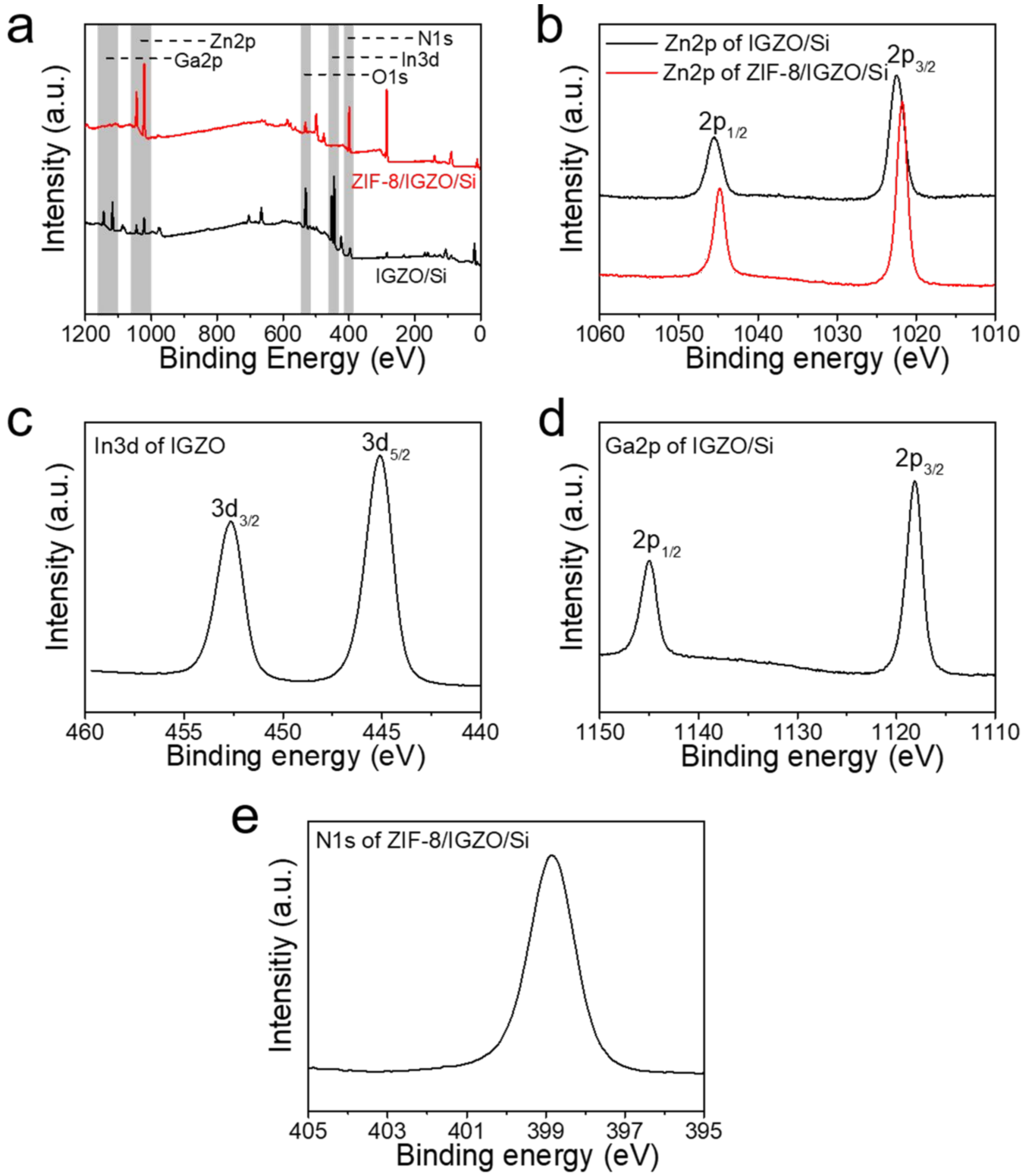

Figure S2. (a) Wide XPS and (b) narrow Zn2p XPS spectra of the IGZO/Si and ZIF-8/IGZO/Si. Narrow (c) In3d and (d) Ga2p XPS spectra of the IGZO/Si. (e) Narrow N1s XPS spectrum of the ZIF-8/IGZO/Si.

An atomic ratio of IGZO was In:Ga:Zn = 0.44:0.37:0.19, which was calculated based on the corresponding peak area of each atom shown in the broad XPS spectrum (Figure S2a). The peak positions of Zn2p$_{1/2}$, Zn2p$_{3/2}$, In3d$_{3/2}$, In3d$_{5/2}$, Ga2p$_{1/2}$, and Ga2p$_{3/2}$ were 1045.5, 1022.35, 452.7, 445.1, 1145.0, and 1118.1 eV, respectively (Figure S2b-d), which are in accord with the reported IGZO XPS peaks.[1] After the ZIF-8 coating, the In3d and Ga2p peaks were disappeared (Figure S2a) and the Zn2p peaks were shifted to the lower binding energy (Figure S2b). In addition, an N1s peak (398.7 eV), representing the imidazolate nitrogen in the ZIF-8, was newly appeared (Figure S2e), demonstrating that the ZIF-8 film covered the IGZO layer.

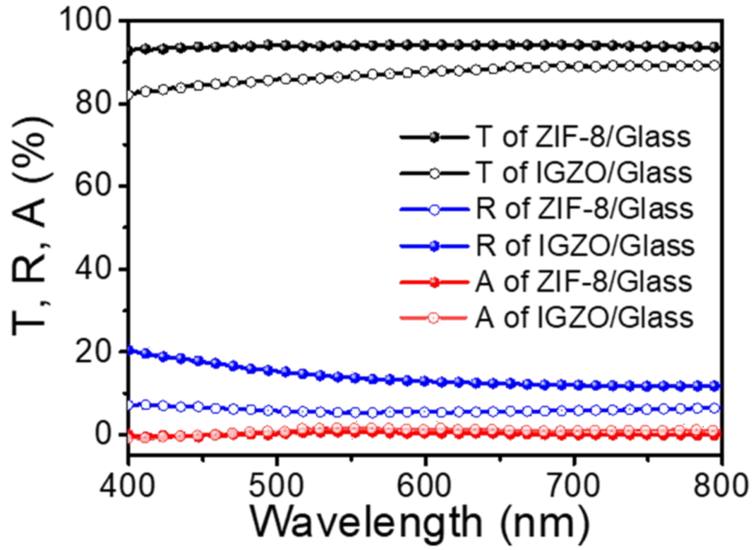

Figure S3. Transmittance (T), reflectance (R), and absorbance of (A) of the ZIF-8/Glass and IGZO/Glass in visible wavelengths.

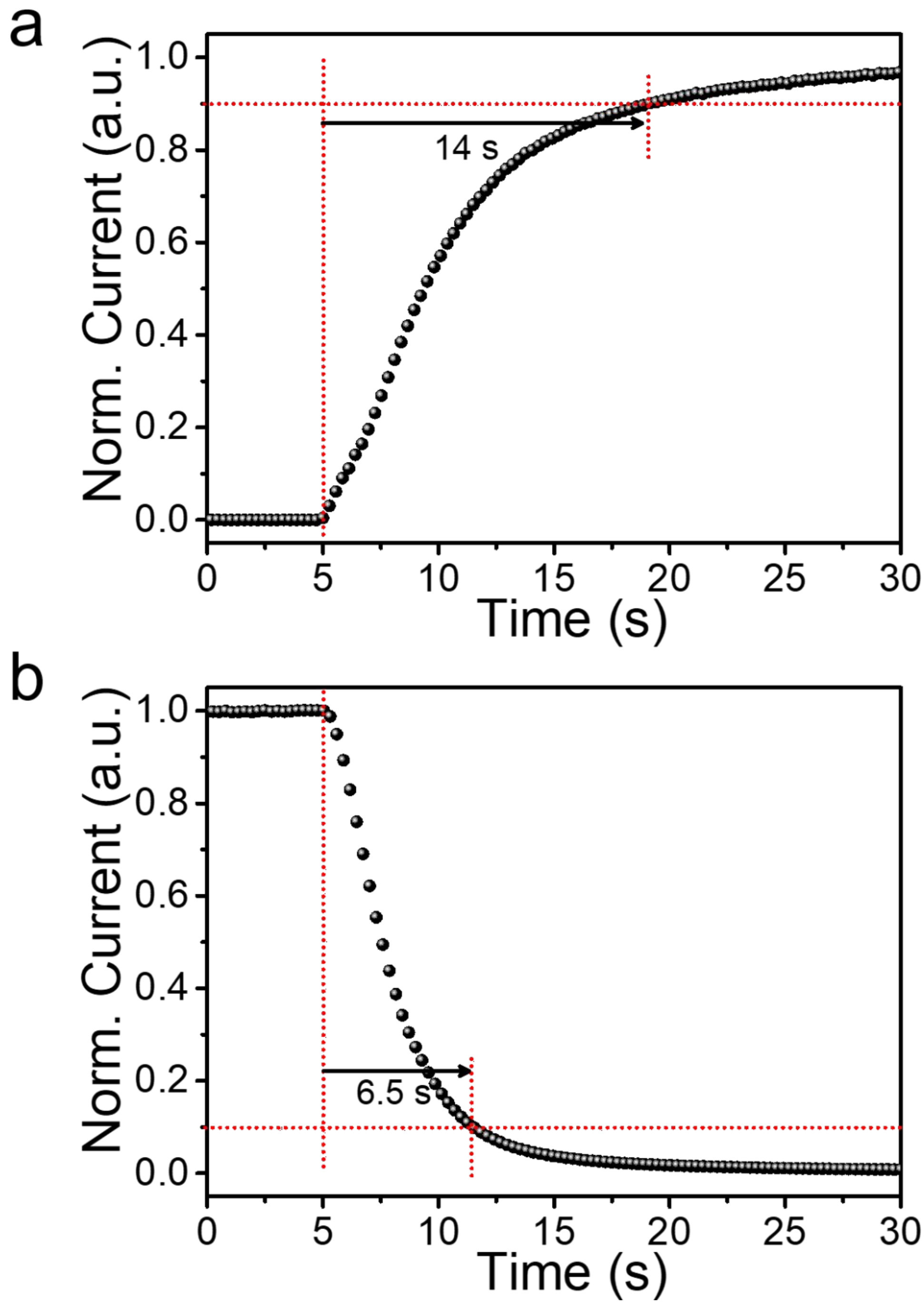

Figure S4. Normalized currents of the ZIF-8/Pd-IGZO sensor during the (a) response, and (b) recovery processes at 1% H_2.

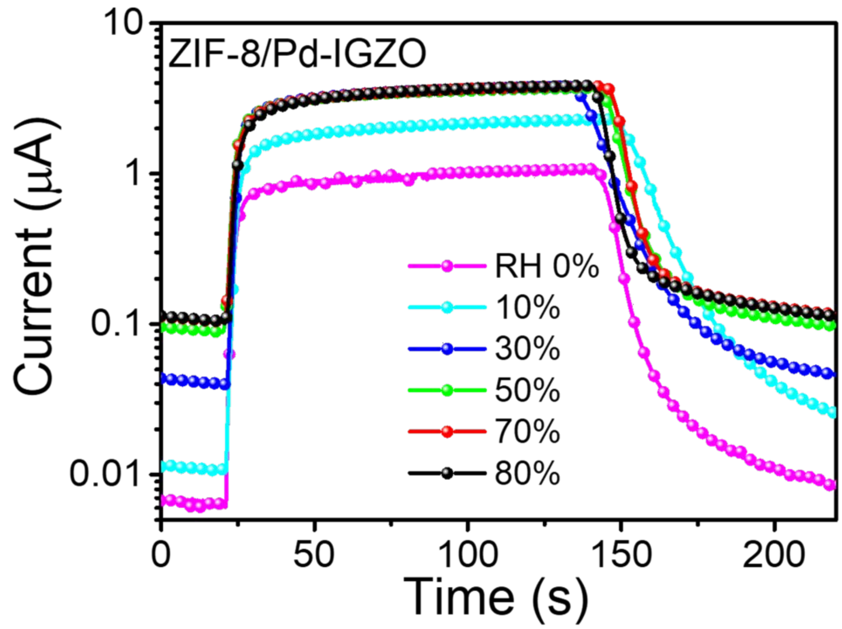

Figure S5. Response curves of the ZIF-8/Pd-IGZO sensor at 1% H_2 under different relative humidity (RH).

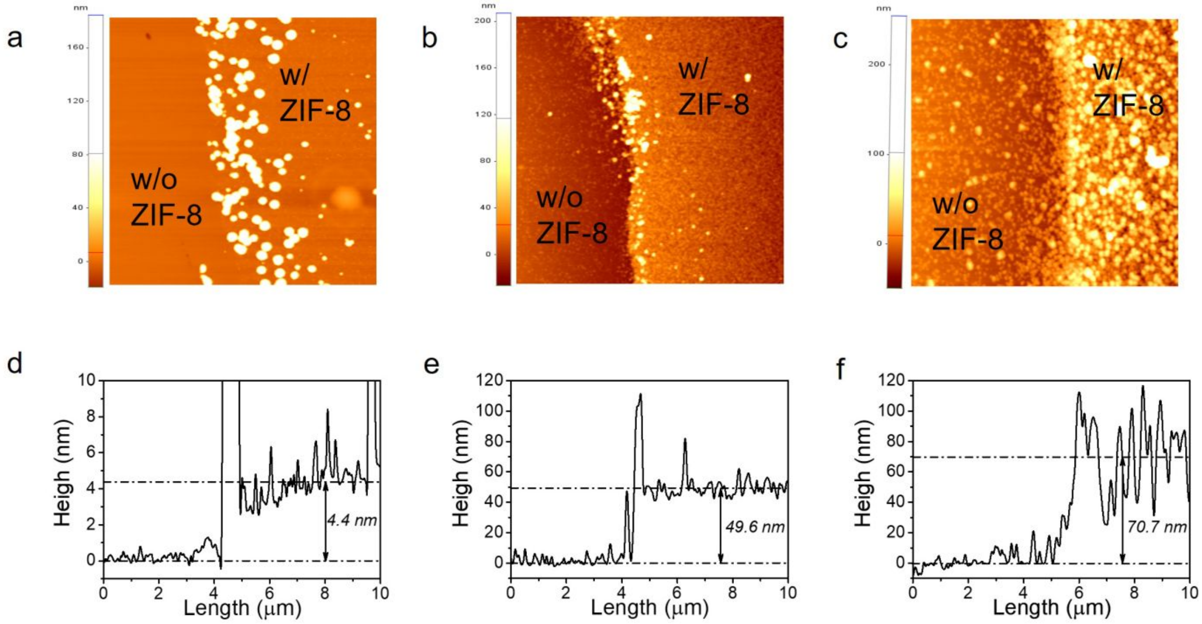

Figure S6. (a–c) AFM mapping results, and (d–f) the corresponding line profiles of the ZIF-8 films with different thicknesses (4.4, 49.6, and 70.7 nm).

The thickness of the ZIF-8 was controlled by varying the concentration of precursors ($Zn(NO_3)_2{\cdot}6H_2O$ and HMIM). We prepared an IGZO-deposited Si substrate, half of which was screened by Kapton tape. The ZIF-8 film was then grown on the substrate. After detaching the tape, AFM analysis was conducted at the edge of ZIF-8 layer.

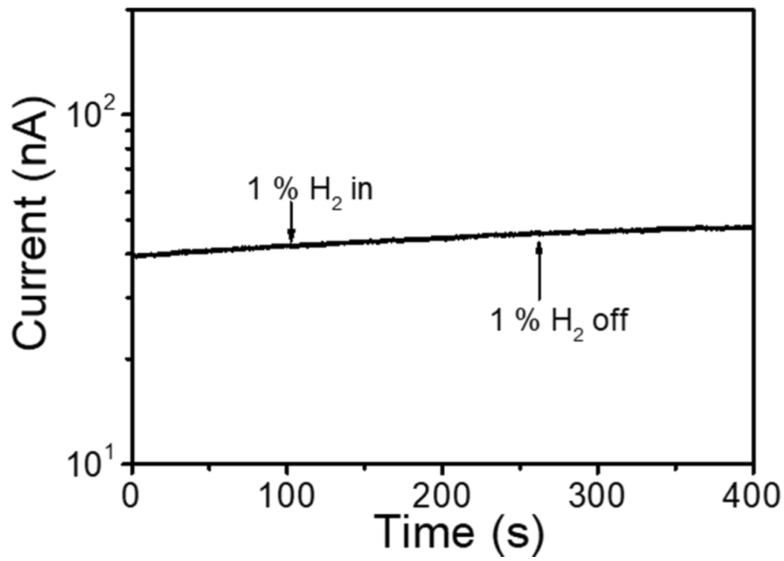

Figure S7. Photocurrent variation of the ZIF-8/IGZO sensor under an irradiance of 5 mW cm^{-2} during the 1% H_2 influx.

Note S1: Langmuir isotherm theory: Adsorption behavior of diatomic H_2 on Pd

The chemisorption of H_2 on a Pd surface is expressed as follows:

$$H_2(g)\text{+}2\text{Pd}(s) \underset{k_{-1}}{\overset{k_1}{\rightleftarrows}} 2\text{H-Pd}(s) \tag{S1}$$

The k_1 and k_{-1} are adsorption and desorption constants, respectively. Based on the formula, the adsorption (r_1) and desorption (r_{-1}) rates are described as

$$r_1 = k_1 p_{H_2}(1-\theta_H)^2 \tag{S2}$$

$$r_{-1} = k_{-1}\theta_H{}^2 \tag{S3}$$

, where P_{H_2} is the partial pressure of H_2, and θ_H is the fraction of occupied adsorption sites on the Pd surface with the dissociated H atoms. Under a steady-state condition in which both reaction rates are equal ($r_1 = r_{-1}$),

$$k_1 p_{H_2}(1-\theta_H)^2 = k_{-1}\theta_H{}^2 \tag{S4}$$

$$\Rightarrow \left(\frac{\theta_H}{1-\theta_H}\right)^2 = \frac{k_1 p_{H_2}}{k_{-1}} \tag{S5}$$

$$\Rightarrow \frac{\theta_H}{1-\theta_H} = \left(\frac{k_1}{k_{-1}}\right)^{1/2} p_{H_2}{}^{1/2} \tag{S6}$$

Assuming a low H_2 concentration that results in a negligible surface coverage θ_H ($\theta_H << 1$), the relation can be approximated as

$$\left(\frac{k_1}{k_{-1}}\right)^{1/2} p_{H_2}{}^{1/2} = \frac{\theta_H}{1-\theta_H} \approx \theta_H \ \Rightarrow \ \theta_H \propto p_{H_2}{}^{1/2} \tag{S7}$$

The proportional expression is valid even if the partial pressure is replaced by the H_2 concentration ($[H_2]$). As the sensing response (R) is directly proportional to the θ_H, the linear relationship between R and $[H_2]^{1/2}$ can be deduced:

$$R \propto \theta_H \propto [H_2]^{1/2} \tag{S8}$$

Note S2: Calibration formula to eliminate the irradiance influence on responsivity

The responsivity of sensor 1 is defined as

$$R_{gas} = \frac{I_1 - I_{1,0}}{I_{1,0}} \times 100\ (\%) \tag{S9}$$

where I_1 and $I_{1,0}$ denote the real-time photocurrent of sensor 1 under ambient conditions, and the base current of sensor 1 with no H_2 atmosphere under unknown irradiance, respectively. As discussed in the manuscript (Figure 4c), both $I_{1,0}$ and the photocurrent of sensor 2 (I_2) can be expressed with empirically defined exponents (α_1 and α_2) and pre-exponential factors (C_1 and C_2) as follows:

$$I_{1,0} = C_1 P^{\alpha_1} \tag{S10}$$

$$I_2 = C_2 P^{\alpha_2} \tag{S11}$$

where P is the irradiance of light. Based on the equations, a mathematical relation between $I_{1,0}$ and I_2 can be deduced.

$$P = \left(\frac{I_{1,0}}{C_1}\right)^{1/\alpha_1} = \left(\frac{I_2}{C_2}\right)^{1/\alpha_2} \tag{S12}$$

$$\Leftrightarrow I_{1,0} = C_1 \left(\frac{I_2}{C_2}\right)^{\alpha_1/\alpha_2} = C I_2^{\alpha} \tag{S13}$$

where C and α represent $C_1 \cdot C_2^{-\alpha_1/\alpha_2}$ and α_1/α_2, respectively. Consequently, by substituting $I_{1,0}$ in Equation (S9) with the form of (S13), the R_{gas} can be calculated with the formula below:

$$R_{gas} = \frac{I_1 - C I_2^{\alpha}}{C I_2^{\alpha}} \times 100\ (\%) \tag{S14}$$

Table S1 Metal nanoparticle-catalyzed H_2 sensors working at room temperature

Sensor	Response (%) @ [H_2]	Response/ Recovery time (s)	Type	Ref.
1 nm Pd-dec IGZO	6.1×10^6 @ 5%	0.3/30	Resistor	2
Pd NWs@ZIF-8_4h	3.47 @ 1%	7/10	Resistor	3
Ni-Pd CS-FET	1383 @ 0.5%	36/62	Transistor	4
Pd nanoparticles@Si nanomesh	27 @ 0.8%	5/13	Resistor	5
Pt/TiO_2/Pt	1.58×10^9 @ 1%	150/280	Resistor	6
Pd/TiO_2 nanotube	5×10^{10} @ 0.1%	-	Resistor	7
Pd-SiNM	764 @ 0.5%	22/-	Schottky diode	8
H_2 CS-FET	600 @ 1%	30/30	Transistor	9
Pd nanotube	3754 @ 1%	210/-	Resistor	10
am-Pd/ZnO NRs	7950 @ 1%	227/95	Resistor	11
Pd-WO_3/graphene/Si	< 50 @ 1%	42/185	Photovoltaic (battery-free)	12
Gr/bluk Si/metal	60 @ 0.1%	>350/900	Photovoltaic (battery-free)	13
Pd/ITO/PET	0.75 @ 1%	1800/900	Triboelectric (battery-free)	14
PDMS/Pd/ZnO NRs	373 @ 1%	100/-	Triboelectric (battery-free)	15
Pd/ZnO NRs/wrinkle patterned PDMS	300 @ 1%	115/126	Triboelectric (battery-free)	16
ZIF-8/Pd-IGZO	**15700 @ 1 %**	**14/7**	**Photovoltaic** (battery-free)	**This work**

References

[1] Chen, J.; Wang, L.; Su, X.; Kong, L.; Liu, G.; Zhang, X. InGaZnO semiconductor thin film fabricated using pulsed laser deposition. *Opt. Express.* **2010**, *18*, 1398-1405.

[2] Kumaresan, Y.; Kim, H.; Jeong, Y.; Pak, Y.; Cho, S.; Lee, R.; Lim, N.; Jung, G. Y. Ultra-high sensitivity to low hydrogen gas concentration with Pd-decorated IGZO film. *IEEE Electron Device Lett.* **2017,** *38*, 1735-1738.

[3] Koo, W.-T.; Qiao, S.; Ogata, A. F.; Jha, G.; Jang, J.-S.; Chen, V. T.; Kim, I.-D.; Penner, R. M. Accelerating palladium nanowire H2 sensors using engineered nanofiltration. *ACS Nano* **2017,** *11*, 9276-9285.

[4] Fahad, H. M.; Gupta, N.; Han, R.; Desai, S. B.; Javey, A. Highly sensitive bulk silicon chemical sensors with sub-5 nm thin charge inversion layers. *ACS Nano* **2018,** *12*, 2948-2954.

[5] Gao, M.; Cho, M.; Han, H. J.; Jung, Y. S.; Park, I. Palladium-decorated silicon nanomesh fabricated by nanosphere lithography for high performance, room temperature hydrogen sensing. *Small* **2018,** *14*, 1703691. DOI: 10.1002/smll.201703691.

[6] Haidry, A. A.; Xie, L.; Wang, Z.; Zavabeti, A.; Li, Z.; Plecenik, T.; Gregor, M.; Roch. T.; Plecenik, A. Remarkable Improvement in Hydrogen Sensing Characteristics with Pt/TiO_2 Interface Control. *ACS Sens.* **2019**, *4*, 2997-3006.

[7] Paulose, M.; Varghese, O. K.; Mor, G. K.; Grimes, C. A.; Ong, K. G. Unprecedented ultra-high hydrogen gas sensitivity in undoped titania nanotubes. *Nanotechnology* **2005,** *17*, 398-402.

[8] Cho, M.; Yun, J.; Kwon, D.; Kim, K.; Park, I. High-Sensitivity and Low-Power Flexible Schottky Hydrogen Sensor Based on Silicon Nanomembrane. *ACS Appl. Mater. Interfaces* **2018,** *10*, 12870-12877.

[9] Fahad, H. M.; Shiraki, H.; Amani, M.; Zhang, C.; Hebbar, V. S.; Gao, W.; Ota, H.; Hettick, M.; Kiriya, D.; Chen, Y.-Z.; Chueh, Y.-L.; Javey, A. Room temperature multiplexed gas sensing using chemical-sensitive 3.5-nm-thin silicon transistors. *Sci. Adv.* **2017,** *3*, e1602557. DOI: 10.1126/sciadv.1602557.

[10] Lim, M. A.; Kim, D. H.; Park, C.-O.; Lee, Y. W.; Han, S. W.; Li, Z.; Williams, R. S.; Park, I. A new route toward ultrasensitive, flexible chemical sensors: metal nanotubes by wet-chemical synthesis along sacrificial nanowire templates. *ACS Nano* **2012,** *6*, 598-608.

[11] Kim, H.; Pak, Y.; Jeong, Y.; Kim, W.; Kim, J.; Jung, G. Y. Amorphous Pd-assisted H_2 detection of ZnO nanorod gas sensor with enhanced sensitivity and stability. *Sens. Actuators, B* **2018,** *262*, 460-468.

[12] Chen, M.; Zou, L.; Zhang, Z.; Shen, J.; Li, D.; Zong, Q.; Gao, G.; Wu, G.; Shen, J.; Zhang, Z. Tandem gasochromic-Pd-WO_3/graphene/Si device for room-temperature high-performance optoelectronic hydrogen sensors. *Carbon* **2018,** *130*, 281-287.

[13] Lee, D.; Park, H.; Han, S. D.; Kim, S. H.; Huh, W.; Lee, J. Y.; Kim, Y. S.; Park, M. J.; Park, W. I.; Kang, C. Y.; Lee, C.-H. Self-Powered Chemical Sensing Driven by Graphene-Based Photovoltaic Heterojunctions with Chemically Tunable Built-In Potentials. *Small* **2019,** *15*, 1804303. DOI: 10.1002/smll.201804303.

[14] Shin, S.-H.; Kwon, Y.; Kim, Y.-H.; Jung, J.-Y.; Nah, J. Triboelectric hydrogen gas sensor with pd functionalized surface. *Nanomaterials* **2016,** *6*, 186. DOI: 10.3390/nano6100186.

[15] Uddin, A. I.; Chung, G.-S. A self-powered active hydrogen gas sensor with fast response at room temperature based on triboelectric effect. *Sens. Actuators, B* **2016,** *231*, 601-608.

[16] Uddin, A. I.; Chung, G.-S. A self-powered active hydrogen sensor based on a high-performance triboelectric nanogenerator using a wrinkle-micropatterned PDMS film. *RSC Adv.* **2016,** *6*, 63030-63036.